scientific reports

Check for updates

OPEN

Optimization of lymphatic drug delivery system with carboplatin for metastatic lymph nodes

Miriu Miyatsu[1], Ariunbuyan Sukhbaatar[1,2,3], Radhika Mishra[1], Arunkumar Dorai[4], Shiro Mori[1,2,3] & Tetsuya Kodama[1,3]✉

Systemic chemotherapy is a common method for treatment of metastatic lymph nodes (LNs), but it has low tissue selectivity and high toxicity. Lymphatic drug delivery system (LDDS) is a novel approach to treat and prevent LN metastases. In a previous study, it was found that the increase of osmotic pressure with varied viscosity of the drug reagent enhances drug retention in the LNs. Here, we optimized the administration conditions to achieve a long-term therapeutic response by varying the dosages and injection rate, using the optimized osmotic pressure and varied viscosity of drug reagent for LDDS. A metastatic LN mouse model was created with MXH10/Mo/lpr mice. Luciferase labelled FM3A mouse mammary carcinoma cells were inoculated in subiliac LN (SiLN) to induce metastasis to the proper axillary LN (PALN). 4 days post tumor cell inoculation, carboplatin (CBDCA) was injected into the tumor-bearing SiLN under different administration conditions. Superior drug retention was observed in the group that received two-doses of CBDCA solution adjusted to an osmotic pressure and viscosity of 1897 kPa and 12 mPa·s, at an injection rate of 10 µL/min. Furthermore, this effect persisted for 42 days. This effect was accompanied by an upregulated expression of CD8, IL-12a, and IFN-γ in the spleen. These results suggest that dual-dose administration at 10 µL/min with hyper-osmotic and high viscosity formulation is optimal and can improve the long-term therapeutic efficacy of LN metastasis.

Keywords Lymph node metastasis, Chemotherapy, Carboplatin, Lymphatic drug delivery system, Osmotic pressure and viscosity

Abbreviations

CBDCA	Carboplatin
cDNA	Complementary deoxyribonucleic acid
D10	Double injection at 10 µL/min
DB	Double bolus injection
dLN	Downstream lymph node
DNA	Deoxyribonucleic acid
EPR	Enhanced permeability and retention
ICG	Indocyanine green
ICP-MS	Inductively coupled plasma mass spectroscopy
IV	Intravenous
IVC	Inferior vena cava
IVIS	In vivo Imaging system
LDDS	Lymphatic drug delivery system
LN	Lymph node
LS	Lymphatic sinus
LV	Lymphatic vessel
MLN	Metastatic lymph node
mRNA	Messenger ribonucleic acid

[1]Laboratory of Biomedical Engineering for Cancer, Graduate School of Biomedical Engineering, Tohoku University, 4-1 Seiryo, Aoba, Sendai, Miyagi 980-8575, Japan. [2]Division of Oral and Maxillofacial Oncology and Surgical Sciences, Graduate School of Dentistry, Tohoku University, 4-1 Seiryo, Aoba, Sendai, Miyagi 980-8575, Japan. [3]Biomedical Engineering Cancer Research Center, Graduate School of Biomedical Engineering, Tohoku University, 4-1 Seiryo, Aoba, Sendai, Miyagi 980-8575, Japan. [4]Institute of Multidisciplinary Research for Advanced Materials, Tohoku University, 2-1-1 Katahira, Aoba, Sendai, Miyagi 980-8577, Japan. ✉email: kodama@tohoku.ac.jp

MS	Marginal sinus
PALN	Proper axillary lymph node
Pt	Platinum
qRT-PCR	Real-Time Quantitative Reverse Transcription Polymerase chain reaction
S10	Single injection at 10 μL/min
SB	Single bolus injection
SiLN	Subiliac lymph node
SV	Subclavian vein
Tc	T cell
Tc1	Type 1 T cell

Lymph node (LN) metastases occur in many types of cancer. Early treatment of LN metastases is essential to prevent distant metastases and reduce mortality[1–4]. Systemic drug delivery strategies fail to effectively treat metastatic LNs (MLNs) due to a number of reasons[5,6]. These include the formation of angiogenesis, partial pressure of oxygen, and perfusion defects within the MLN, which itself is an organ with an abundant vascular network that does not change partial pressure of oxygen as metastatic cells proliferate, replacing parenchyma with tumor tissue without forming new tumor vessels[7,8]. Therefore, in MLNs, accumulation of high-molecular-weight anticancer drugs by the enhanced permeability and retention (EPR) effect does not occur when administered intravenously. Therefore, we developed a new drug delivery method that does not rely on the hematogenous route, the lymphatic drug delivery system (LDDS). The LDDS entails injection of the drug formulation directly into the LN for delivery into it and its downstream LN (dLN) to prevent and treat LN metastasis. LDDS significantly enhances drug delivery and retention in the metastatic LN[9–11] and thus significantly suppresses tumor growth, compared to intravenously administered chemotherapy. In using LDDS, parameters that can amplify the therapeutic response are formulation osmotic pressure and viscosity, the injection rate, and the number of dosages. Recent studies, using chemotherapeutic agent cisplatin (CDDP), DTX, etc., have revealed that the optimal range of osmotic pressure and viscosity for LDDS is approximately 1000 ~ 3000 kPa and 1 ~ 12 mPa·s[12–15].

The present study focuses on carboplatin (CBDCA), because[16–18] while CBDCA and CDDP have comparable antitumor effects against cancer, CBDCA has greatly reduced systemic toxicity, such as nephrotoxicity, neurotoxicity, and ototoxicity, in comparison to CDDP[18–20]. Importantly, CBDCA also has good osmotic and viscosity suppressant properties. Unlike CDDP, CBDCA can be dissolved in both glucose and polysorbate while retaining its cytotoxic activity, allowing evaluation of the drug's efficacy under conditions where it is dissolved in a formulation containing both as major components. Another important factor is the effect of carboplatin on the immune system. Recent studies have shown that CBDCA has potential to induce immunogenic cell death (ICD), in the process of causing DNA inhibition[21]. Since the plasma half-life is independent of the dose[22], we believe that varying the osmotic pressure, viscosity, and number of dosages can change the CBDCA half-life and approach both cytotoxicity and anti-tumor immunity, thereby enhancing long-term anti-tumor effects. However, the long-term therapeutic efficacy has not been investigated when the injection rate and number of doses are varied using a solvent adjusted to this optimal osmotic pressure and viscosity. Therefore, the purpose of this study was to evaluate the administration conditions to sustain the therapeutic effect for a long period of time using a solvent with an optimized osmolarity with varied viscosity (Fig. 1).

Results

Evaluation of drug delivery and retention using in vivo ICG biofluorescent intensity measurement

In all groups, the ICG solution administered in SiLN was delivered to the downstream LN, PALN through lymphatic vessel (Fig. 2A). The low-viscosity (1 mPa·s) formulation adjusted by glucose, injected by bolus (1897G SB group), was delivered instantaneously to the PALN. The high-viscosity (12 mPa·s) formulation adjusted by polysorbate, injected by bolus (1897P SB), showed higher ICG accumulation in the SiLN and lesser in PALN. The group of high-viscosity (12 mPa·s) formulation injected at 10 μL/min (1897P S10) achieved the best delivery in both SiLN and PALN in this study. In mice that received two doses of high viscosity formulation injected by bolus (1897P DB group), mass of tumor was formed between SiLN and PALN and caused to lymphatic blockage after day 21 (Table 1). However, when the same formulation was administered at 10 μL/min (1897P D10 group), no lymphatic blockage formed, and the highest ICG retention was received in SiLN and PALN up to day 42 (Fig. 2B–E). This result showed no significant difference from the group that received a single dose of the same solvent (1897P S10 group) at day 42; however, a trend toward increased retention volume with two doses was observed. With quantification of 195Pt using ICP-MS using tumor-free mice (Table 2), the highest concentration of Pt was 774 ng/L for the SiLN of 1897G S10 on the day of treatment ($D0^T$), whereas 442.8 ng/L for 1897P S10 ($D0^T$). On $D0^T$, accumulation of Pt was found to be high in the kidney and liver among the other organs in both groups. Nine days after the treatment ($D9^T$), a higher concentration of Pt was found in the liver and lung of 1987G S10, followed by SiLN. In the 1897P S10 group, the highest concentration was found in liver, kidney, and SiLN. Overall, a higher retention rate was detected in the 1897P S10 group than in the 1897G S10 group.

Evaluation of tumor growth using in vivo bioluminescent intensity measurement

The in vivo bioluminescent intensity in SiLNs and axillar regions including metastatic PALNs increased over the time until day 42 in all experimental groups (Fig. 3 A, B and D). In the group of 1897P D10, the in vivo bioluminescent intensity was significantly reduced until day 18 compared to Placebo group (Fig. 3 C and E). Thereafter, tumor cells in SiLN and PALNs increased over time until day 42, as evidenced by the increasing bioluminescent intensity but still remained the lowest among all experimental groups (Fig. 3C, E).

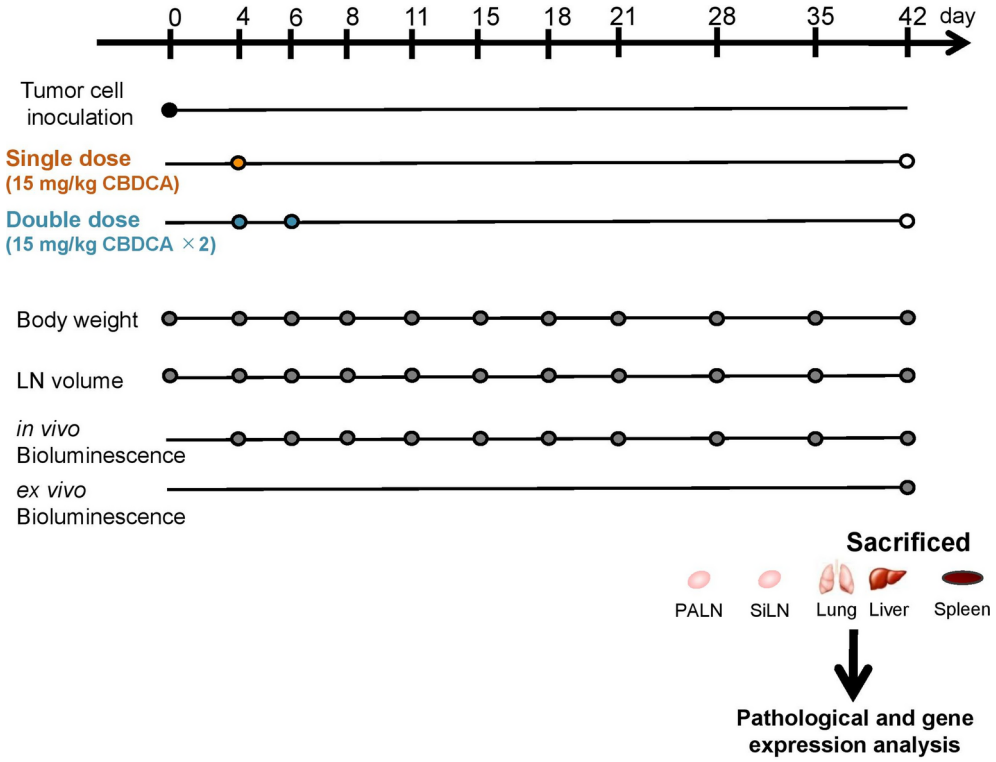

Fig. 1. Treatment schedule and tumor growth and side effect evaluation days.

Evaluation of metastatic LN volume changes

SiLN volume increased dramatically in Placebo and 1897G SB groups but stayed fairly constant/increased only slightly in groups that received two dosages, 1897G DB and 1897P D10 groups (Fig. 4A). LN volume changes in PALN did not drastically differ between all experimental groups or change across time but was the smallest in the 1897P D10 group on day 42 (Fig. 4B, C).

Evaluation of ex vivo bioluminescent intensity and histopathological analysis

The ex vivo bioluminescence in PALN on day 42 showed strong bioluminescent intensity on the SiLN and PALN in the Placebo group and only partially existed in the 1897G SB group (Fig. 5A). The lowest mean bioluminescent intensity was detected in the SiLN and PALN in 1897P D10 group (Fig. 5B). The lungs of all mice in the Placebo group showed strong bioluminescent intensity (Fig. 5A, B). In contrast, the lungs of mice in the 1897G SB had significantly lower bioluminescent intensity than the Placebo group (Fig. 5B). The mice in 1897P D10 group showed individual differences in lung bioluminescent intensity, with 3 out of 5 mice showing high level (Fig. 5B). Overall survival was found to be 50.0% in 1897G SB, 1897G DB, 1897P S10 and 1897P D10 groups (Fig. 5C). Overall survival benefits did not have any direct correlation with treatment efficacy.

The results of histopathological analysis of SiLN and PALN in Placebo, 1897G SB, 1897G DB, and 1897P D10 groups are shown in Fig. 6. In the HE-stained specimen of SiLN, the entire LN was filled with tumor cells in Placebo group, and the parenchyma was replaced by tumor cells in all mice (Fig. 6(A) a, b). In 1897G SB and 1897G DB groups, tumor cells occupied a relatively large area of the LN (Fig. 6(A) c ~ f). On the other hand, similar to the ex vivo bioluminescence intensity results, three out of five mice in 1897P D10 group showed low tumor growth grades of 0 ~ 1, indicating a narrow range of tumor cells in the SiLNs (Fig. 6(A) q ~ h, Fig. 6C).

In PALN HE-stained specimen, the tumor growth grade within the LN was higher in Placebo and 1897G DB groups (Fig. 6A, D). In contrast, no tumor cells were observed in the LN of all mice in the 1897P D10 group, and the tumor growth grade was 0 (Fig. 6D).

Quantitative RT-PCR analysis

The Fig. 7 shows the mRNA expression levels of cell surface antigens (CD4, CD8) and cytokines (IL-6, IL-12 β , IL-12 α, TNF-α, IFN-γ) measured by quantitative RT-PCR in the spleens excised from treated mice. Among them, the Fig. 7A shows the group sampled on day 10, and the Fig. 7B shows the group sampled on day 42. On day 42, the expression levels of CD8, IL-10, IFN-γ and IL12-α were the highest in the 1897P D10 group and were increased compared to the Placebo group. Among them, IL-12 α was statistically significantly increased compared to 1897G SB group. On the other hand, the expression levels of IL-6, CD4, and TNF-a were decreased compared to the Placebo group. On day 10, the expression levels of CD4, CD8, IL-10, TNF-α, IL-12 β and IFN-γ were increased in the 1897P D10 group compared to the Placebo and 1897P S10 groups. Notably, CD4, CD8,

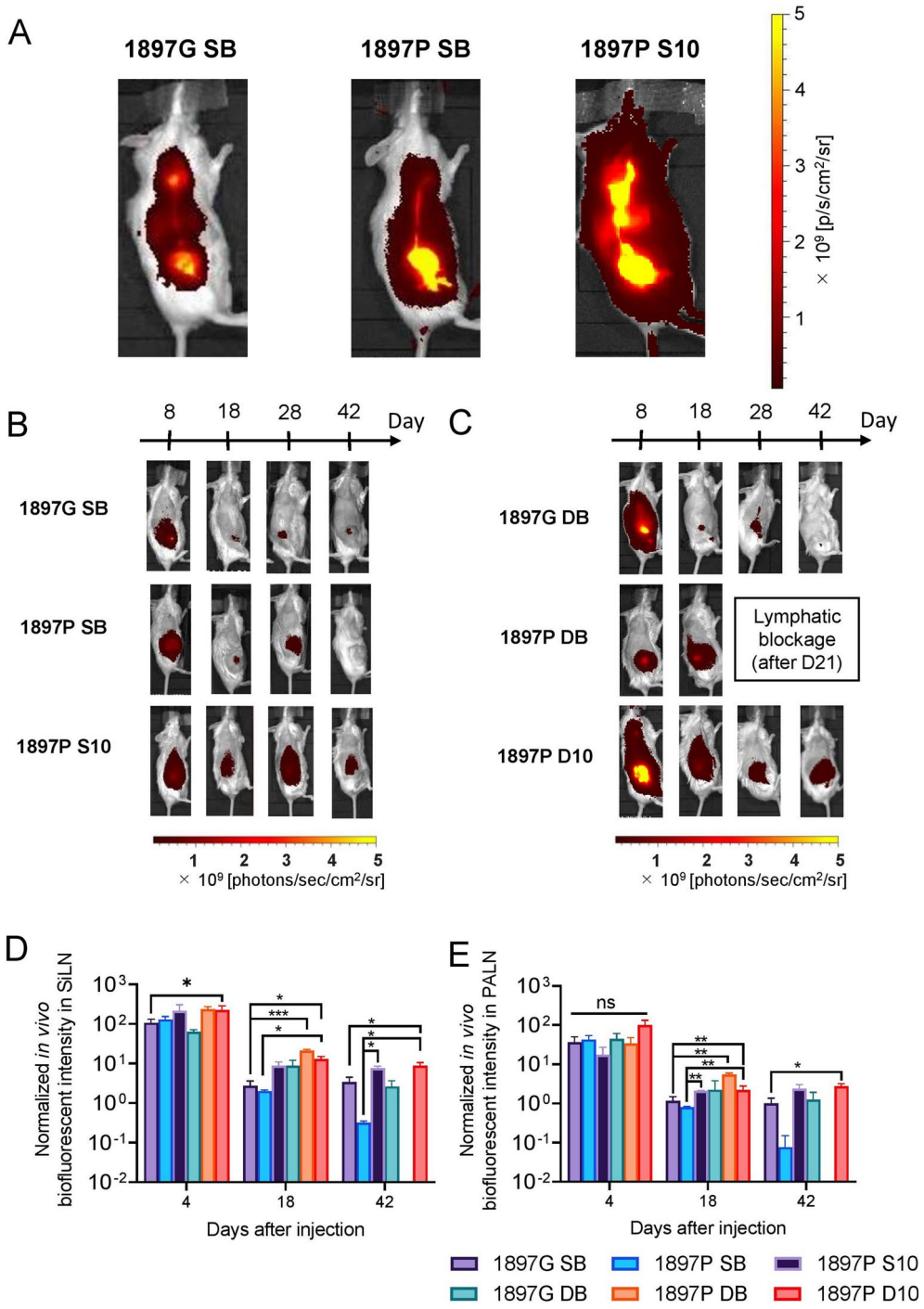

Fig. 2. Drug delivery under different dosing conditions. (**A**) Representative ICG fluorescence intensity images immediately after administration of each dose group. 1897G SB: in vivo ICG fluorescence intensity image immediately after LDDS bolus administration of ICG solvent with osmotic pressure of 1897 kPa and viscosity of 1 mPa-s to SiLN, 1897P SB: in vivo ICG fluorescence intensity image immediately after LDDS bolus administration of ICG solvent with osmotic pressure of 1897 kPa and viscosity of 12 mPa·s to SiLN. 1897P S10: in vivo ICG fluorescence intensity image immediately after LDDS administration of ICG solvent with osmotic pressure of 1897 kPa and viscosity of 12 mPa·s at 10 µL/min to SiLN. (**B**) Representative in vivo ICG fluorescent images in the single-dose group. (**C**) Representative in vivo ICG fluorescent images in the double-dose group. (**D**) in vivo ICG fluorescence intensity changes in SiLN on days 4, 18 and 42. 1897G SB, n = 4, 1897P SB, n = 2, 1897P S10, n = 2, 1897G DB, n = 5, 1897P DB n = 5, 1897P D10, n = 5. Mean ± S.E.M. ns, nonsignificant. (**E**) in vivo ICG fluorescence intensity changes in PALN on days 4, 18 and 42. 1897G SB, n = 4, 1897P SB, n = 2, 1897P S10, n = 2, 1897G DB, n = 5, 1897P DB n = 5, 1897P D10, n = 5. Mean ± S.E.M. ns, nonsignificant.

Experimental group	Osmotic pressure [kPa]	Viscosity [mPa·s]	Number of dosages
1897G SB	1897	1	1
1897G DB			2
1897P SB		12	1
1897P S10			1
1897P DB			2
1897P D10			2

Table 1. Experimental groups and different dosing conditions in this study. Placebo group ($n = 11$), 1897G SB (one dose of solvent with an 1897 kPa of osmotic pressure and 1 mPa ● s of viscosity at bolus) group ($n = 8$), 1897G DB (two doses of solvent with an 1897 kPa of osmotic pressure and 1 mPa ● s of viscosity at bolus) group ($n = 10$), 1897P SB (one dose of solvent with an 1897 kPa of osmotic pressure and 12 mPa ● s of viscosity at bolus) group ($n = 5$), 1897P S10 (one dose of solvent with an 1897 kPa of osmotic pressure and 12 mPa ● s of viscosity at 10 μL/min) group ($n = 4$), 1897P DB (two doses of solvent with an 1897 kPa of osmotic pressure and 12 mPa ● s of viscosity at bolus) group ($n = 10$), 1897P D10 (two doses of solvent with an 1897 kPa of osmotic pressure and 12 mPa ● s of viscosity at 10 μL/min) group ($n = 10$).

Pt concentration (ng/L)	1897G S10 ($D0^T$)	1897G S10 ($D9^T$)	1897G S10 retention	1897P S10 ($D0^T$)	1897P S10 ($D9^T$)	1897P S10 retention
SiLN	774.0 (172.3)	1.9 (0.8)	0.25%	442.8 (354.0)	9.3 (2.0)	2.1%
PALN	32.9 (13.0)	0.4 (0.4)	1.2%	16.9 (4.1)	5.4 (0.2)	32.0%
Lung	49.2 (1.2)	3.2 (2.5)	6.5%	14.6 (5.0)	6.5 (0.1)	43.8%
Liver	262.4 (41.8)	8.0 (7.0)	3.0%	201.1 (31.2)	30.1 (2.9)	15.0%
Kidney	654.9 (133.6)	0.2 (3.0)	0.03%	165.8 (60.4)	12.5 (2.8)	7.5%

Table 2. Accumulation and retention of Carboplatin using ICP-MS based on Platinum (Pt) concentration. Data given as mean (SEM). Carboplatin in 1897 kPa osmotic pressure with different viscosity solutions injected via LDDS on Day 0 ($D0^T$). Platinum concentration in the SiLN, PALN, lung, liver and kidney were quantified on day 0 and/or day 9 after injection of Carboplatin using ICP-MS. Platinum retention in per organs were calculated with $D0^T/D9^T$*100. 1897G S10 ($D0^T$), n = 3; 1897G S10 ($D9^T$), n = 3; 1897P S10 ($D0^T$), n = 3; 1897P S10 ($D0^T$), n = 2.

IL-10, TNF-α and IL-12 β were statistically significantly increased compared to 1897P S10 group in the 1897P D10 group.

Discussion

This study underscores the importance of drug retention in the therapeutic efficacy of carboplatin when administered via LDDS (Lymphatic Drug Delivery System) for treating metastatic lymph nodes (LNs). Our results show that the 1897P D10 group demonstrated significantly higher drug retention in SiLN, PALN, liver, lung, and kidney, suggesting that increasing drug retention can enhance its therapeutic efficacy. Specifically, we observed that higher drug retention was associated with lower tumor progression and reduced bioluminescence intensity in the SiLN and PALN. This finding highlights that improved drug retention within the lymphatic system plays a critical role in optimizing treatment outcomes for metastatic LNs.

Furthermore, the in vivo bioluminescence intensity measurements indicate that the anti-tumor effect was not solely dependent on the amount of drug administered but also on how effectively the drug remained in the target areas. The fact that the 1897P D10 group exhibited lower tumor grades and reduced bioluminescence intensity compared to the 1897G DB group, which suggests that even small adjustments in drug delivery parameters, such as viscosity and injection rate, can have significant therapeutic implications. Despite substantial individual variation for the 1897P D10 group, the therapeutic effect tended to improve with two doses. Furthermore, based on the results of Fig. 7, we consider it reasonable that individual differences occur, as immune-related factors also change with two doses.

One of the most notable findings in this study was the influence of injection rate and viscosity on drug retention. Specifically, the 10 μL/min injection rate, when paired with the high-viscosity formulation, resulted in significantly lower in vivo bioluminescence intensity in the SiLN and PALN. This suggests that modifying the drug delivery conditions can effectively prolong drug retention and enhance therapeutic efficacy, even without increasing the overall drug dose.

Dosing at 10 μL/min was effective in high-viscosity solvents because of its superior delivery compared to bolus administration. Our previous study using fluorescent dyes to compare drug delivery to downstream LNs

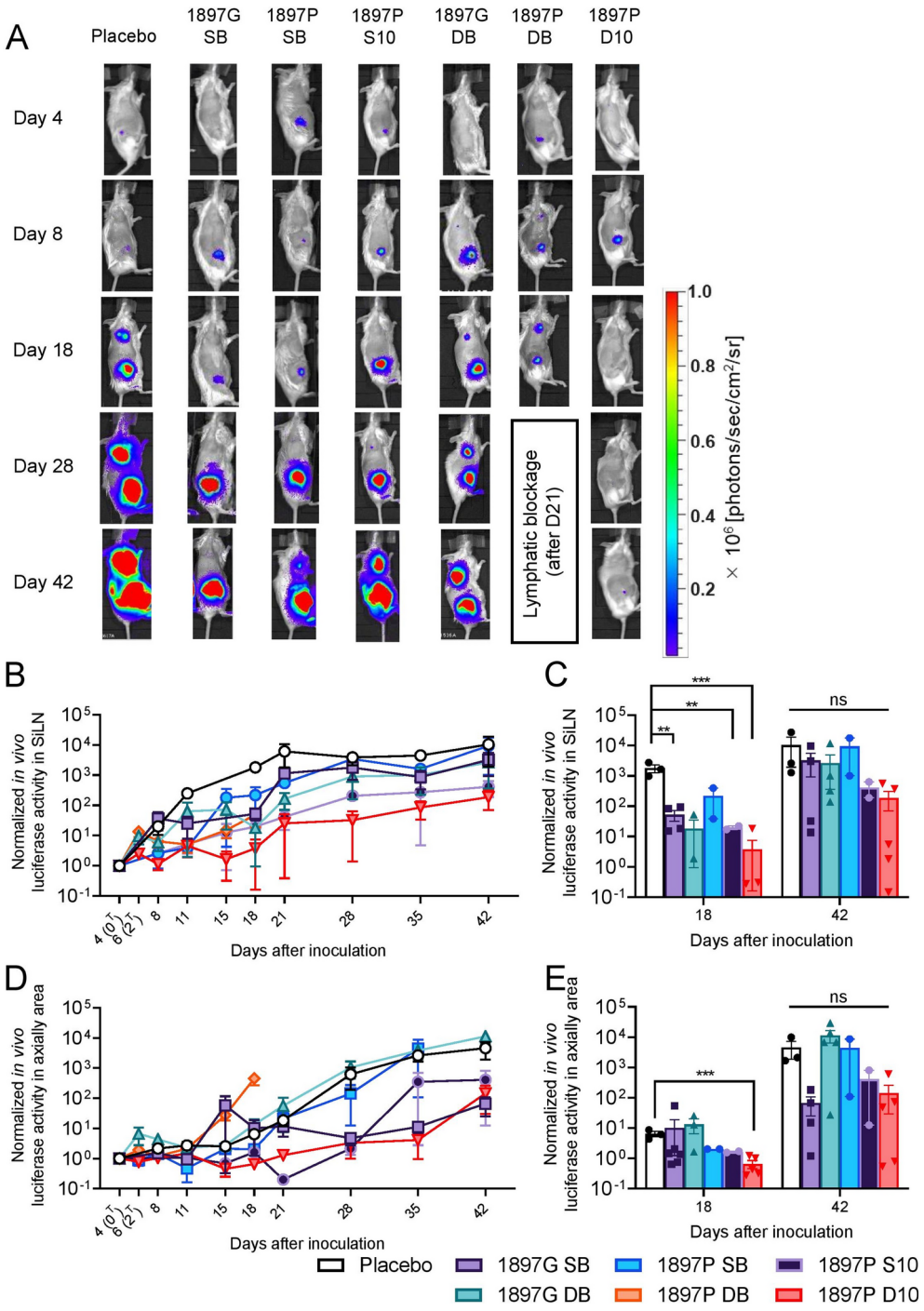

Fig. 3. Antitumor effect on metastatic LN. (**A**) Representative in vivo bioluminescent images. (**B**) in vivo bioluminescence intensity normalized by Day 4 in SiLN. (**C**) Normalized in vivo bioluminescence intensity of SiLN at days 18 and 42. Placebo, n = 3; 1897G SB, n = 4; 1897P SB, n = 2; 1897P S10, n = 2; 1897G DB, n = 5; 1897P DB n = 5; 1897P D10, n = 5. Mean ± S.E.M. ns, not significant. (**D**) in vivo bioluminescence intensity normalized by Day 4 in PALN. (**E**) Normalized in vivo bioluminescence intensity of PALN at days 18 and 42. Placebo, n = 3; 1897G SB, n = 4; 1897P SB, n = 2; 1897P S10, n = 2; 1897G DB, n = 5; 1897P DB n = 5; 1897P D10, n = 5. Mean ± S.E.M. ns, not significant.

at 10 μL/min and bolus administration showed that the mean fluorescence intensity in downstream LNs was significantly higher in 10 μL/min than bolus administration[27]. Moreover, at the 10 μL/min injection rate, the fluorescence intensity in the dLN, PALN increased as the drug volume infused into the upstream LN, SiLN, whereas the bolus administration remained consistently low. Thus, the low injection rate ensured delivery to the dLNs, and the internal penetration of the drug inhibited lymphatic and vascular drainage, contributing to its retention. On the other hand, in the group that received two bolus injections of the same solvent with an

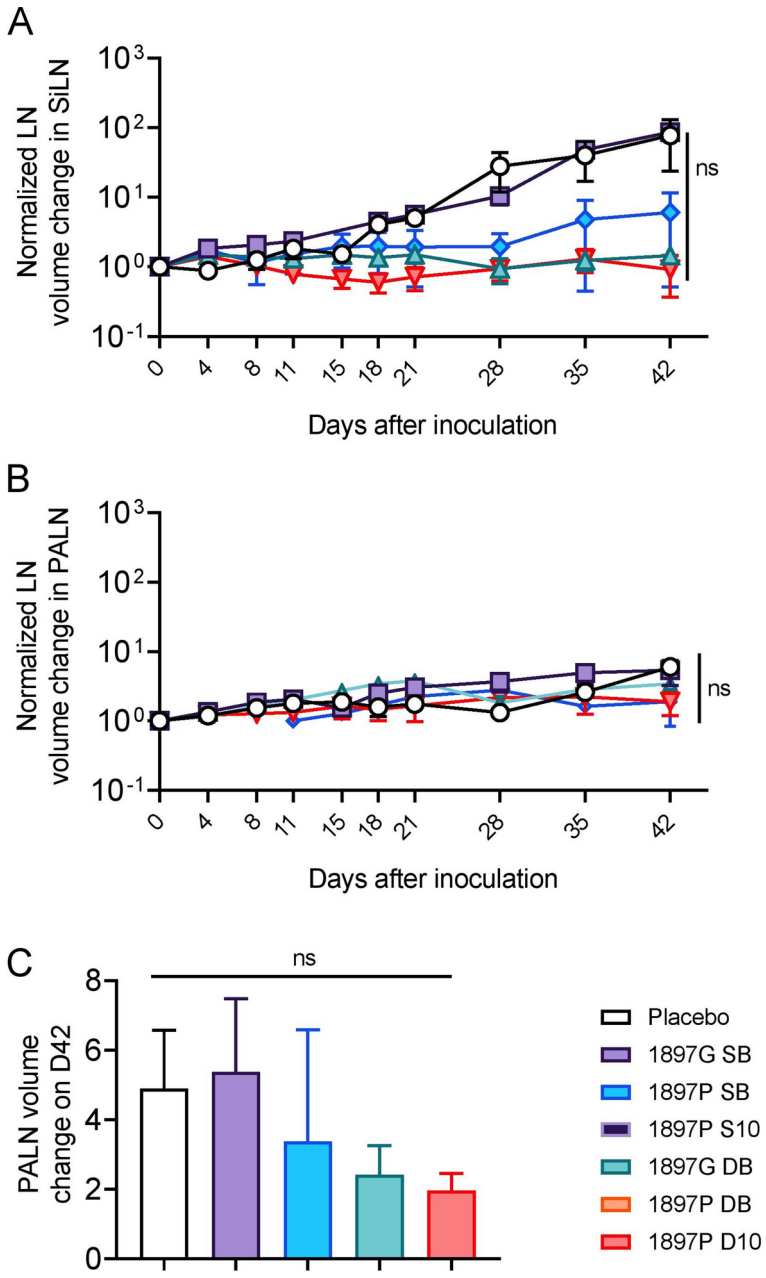

Fig. 4. LN volume changes. (**A**) Normalized LN volume changes in SiLN. (**B**) Normalized LN volume changes in PALN. (**C**) PALN volume changes on day 42 in PALN.

osmotic pressure of 1897 kPa and viscosity of 12 mPa·s (1897P DB group), tumor growth was observed in the lymph vessels on Day 21 and formation of tumor mass was confirmed. This suggests that two dosages of bolus administrations of a hyper osmotic and high viscosity formulation are not an appropriate condition for clinical use.

Quantitative PCR results on day 42 showed that CD4 expression was relatively low, while CD8 and IFN-γ expression was high in the 1897P D10 group, which had the best response to treatment (Fig. 7A). These results suggest that systemic anti-tumor immunity was activated by CBDCA increasing in IFN-γ from $CD8^+$ T cells rather than $CD4^+$ T cells. $CD8^+$ and $CD4^+$ T cells are responsible for directing the overall immune response and directly killing tumor cells. These functions are usually mediated by $CD4^+$ and $CD8^+$ T cells, among which $CD8^+$ T cells generally secrete high levels of IFN-γ and act to kill tumor cells and infected cells. Several Tc subsets with different functions have been identified in $CD8^+$ T cells, and each $CD8^+$ T cell subset has a different role in anti-tumor immune responses[28].

Among them, Tc1 cells, in which $CD8^+$ T cells are differentiated by IL-12α, produce more IFN-γ and TNF-α and have a role in efficiently killing tumor cells[29–31].

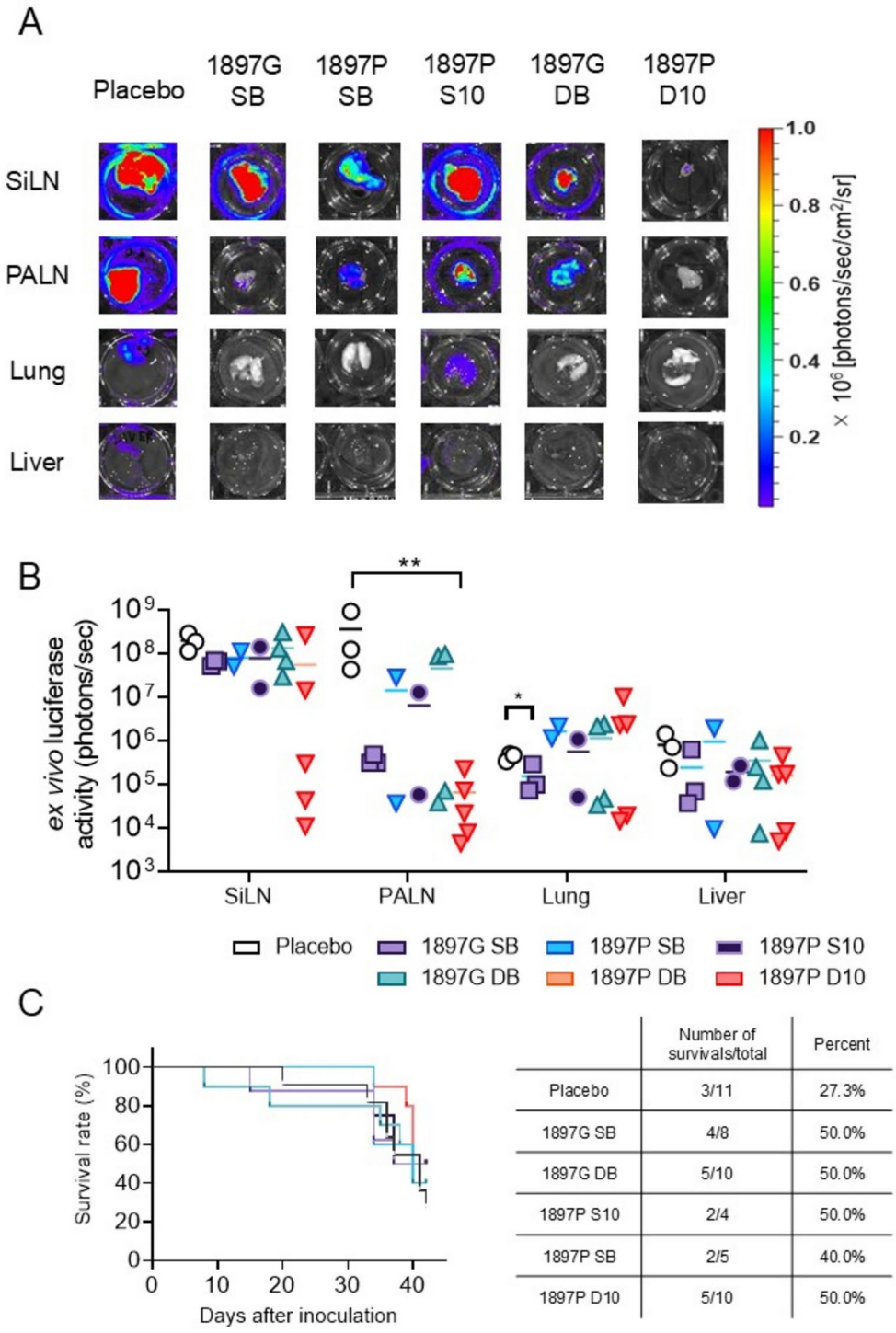

	Number of survivals/total	Percent
Placebo	3/11	27.3%
1897G SB	4/8	50.0%
1897G DB	5/10	50.0%
1897P S10	2/4	50.0%
1897P SB	2/5	40.0%
1897P D10	5/10	50.0%

Fig. 5. ex vivo bioluminescent intensity. (**A**) Representative ex vivo bioluminescence images of SiLN, PALN, lung and liver. (**B**) ex vivo bioluminescence intensity in SiLN, PALN, lung and liver. Placebo group, n = 3; 1897G SB group, n = 4; 1897P SB group, n = 2; 1897P S10 group, n = 2; 1897G DB group, n = 5; 1897P D10 group, n = 5. (**C**) Overall survival rate.

In this study, CD8 and IFN-γ expression was higher in the 1897P D10 group, suggesting that $CD8^+$ T cells were the major factor (Fig. 7B). In the treated groups, $CD8^+$ T-cell expression increased as the time of drug retention in the LN increased (Fig. 7B). These results suggest that the drug retention time in the LN is related to the expression level of $CD8^+$ T cells in spleen. Therefore, CD8 expression was highest in the 1897P D10 group, which had the longest drug retention time in the LN, and CD8 expression was lowest in the 1897G SB group, which had the shortest drug retention in the LN. On the other hand, the 1897P D10 group showed high expression of IL-10, which is indicative of an immune tolerance response (Fig. 7B). This may be due to the increased

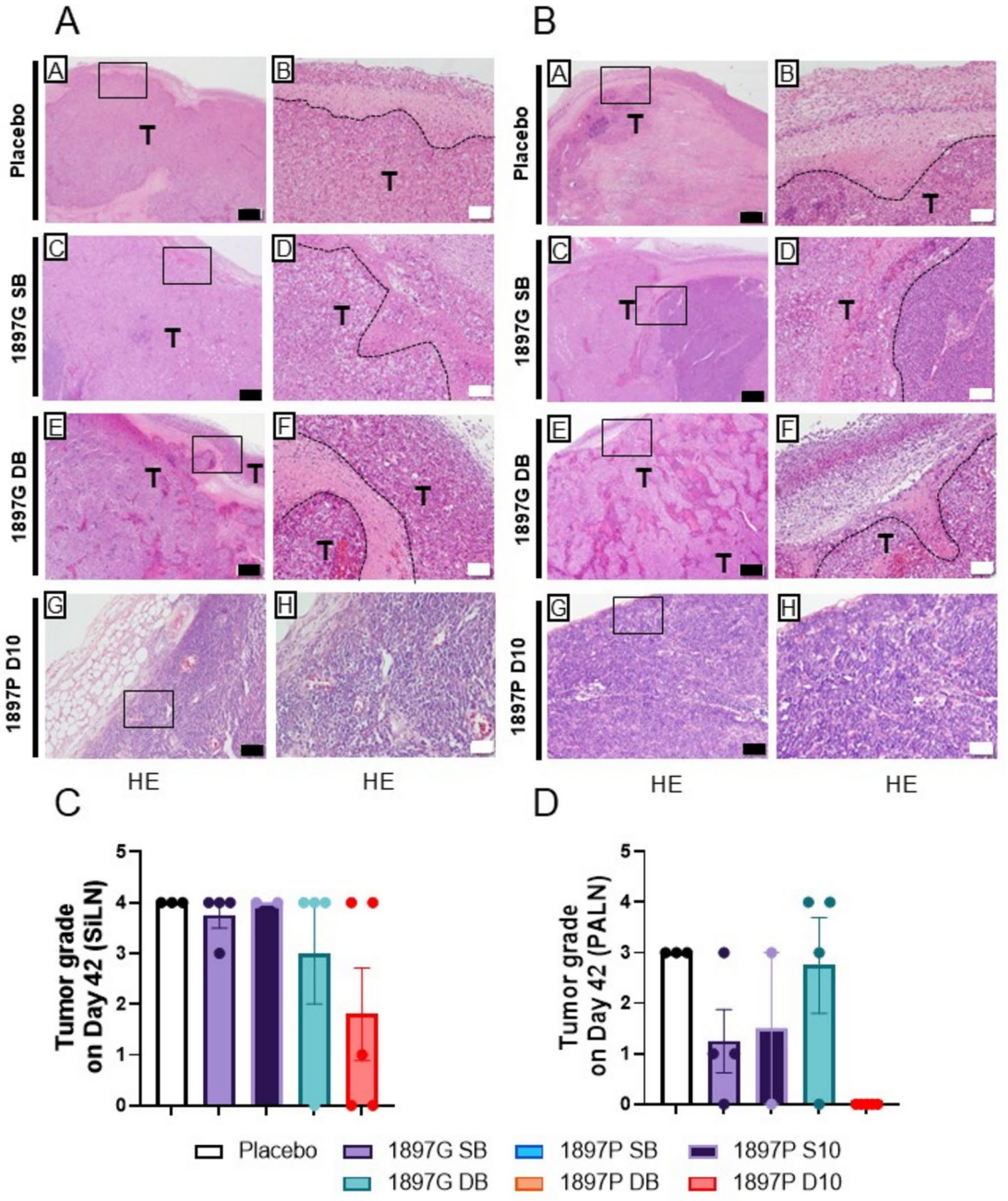

Fig. 6. HE stained histopathological images. (**A**) Representative HE stained histopathological images of SiLN. (a, b) Placebo group, (c, d) 1897G SB group, (e, f) 1897G DB group, (g, h) 1897P D10 group. b, d, f, h are magnified views of the regions indicated by a, c, e, g, respectively. T: tumor, Scalebar: black, 200 μm; white, 50 μm. (**B**) Representative HE stained histopathological images of PALN. (a, b) Placebo group, (c, d) 1897G SB group, (e, f) 1897G DB group, (g, h) 1897P D10 group. b, d, f, h are magnified views of the regions indicated by a, c, e, g, respectively. T: tumor, Scalebar: black, 200 μm; white, 50 μm. (**C**) Tumor growth grade in SiLN by histopathological analysis. (**D**) Tumor growth grade in PALN by histopathological analysis.

expression of IFN-γ, which suppresses the excessive immune-promoting response and maintains the balance of the body's immune system. Furthermore, a recent study reported that CBDCA activates the NF-κB pathway, which plays a central role in immune responses, and increases IL-6 production through DNA damage induced by platinum drugs[32]. These findings are consistent with the quantitative PCR results in this study, suggesting that CBDCA is involved in antitumor immunity. However, it is known that chemotherapy treatment of tumors producing IL-6 prior to therapeutic intervention results in a more pronounced bias of monocyte differentiation toward tumor-promoting M2-like macrophages, leading to a higher production of IL-10 and a decrease in IL-

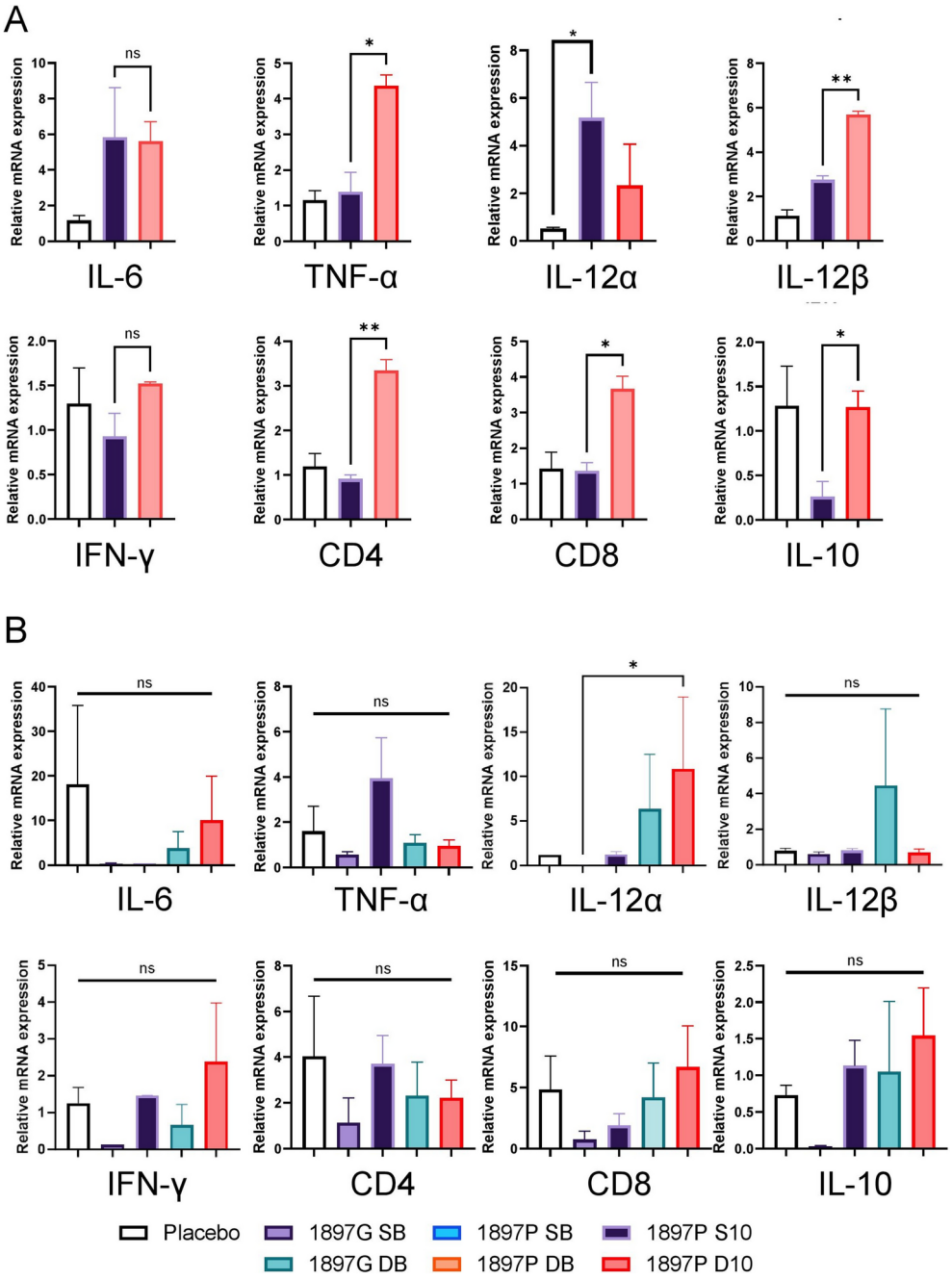

Fig. 7. Quantitative RT-PCR analysis. (**A**) Expression levels of cell surface antigens and cytokines in spleen at day 10. IL-6, TNF-α, IL-12α, IL-12β, IFN-γ, CD4, CD8 and IL-10 in CBDCA group were upregulated compared to Placebo group. The upregulation of TNF-α, IL-12α, IL-12β, CD4, CD8 and IL-10 in 1897P D10 group being especially significant. (**B**) Expression levels of cell surface antigens and cytokines in spleen at day 42. IL-6, IL-12α, IFN-γ, CD8 and IL-10 were upregulated in 1897P D10 group and IL-12α being especially significant.

12 production, and enhanced resistance to chemotherapy known[32]. In the early stages, the 1897P D10 group showed increased levels of IL-6, TNF-α, IL-12β, IFN-γ, CD4, and CD8, indicating an initial immune response against tumor progression. This likely involved pro-inflammatory cytokines and T cell responses. In later stages, the 1897P D10 group exhibited elevated levels of IL-6, IL-12α, IFN-γ, CD8, and IL-10 on day 42, suggesting a sustained or evolving immune response. This phase may involve ongoing T cell activation, regulation of immune responses (IL-10), and potentially a shift towards a more balanced immune profile with decreased TNF-α, IL-12β, and CD4. Therefore, examination of the intratumoral microenvironment will be needed before therapeutic intervention with platinum drugs.

This is the first study to quantitatively demonstrate the relationship between the long-term therapeutic effect on metastatic LNs and the administration conditions. However, the dosing schedule to achieve a greater therapeutic efficacy on metastatic LNs is not yet perfect and needs further investigation.

Based on the results of previous studies, we investigated the importance of osmotic pressure and viscosity adjusted formulation in the LDDS treatment of metastatic LNs and the therapeutic efficacy of multiple dosages of hyper osmotic and high viscosity and injection rate to improve the long-lasting effect.

Material and Methods

Mice

MXH10/Mo/lpr mice, are recombinant inbred strains originating from MRL/MpJ-*lpr*/*lpr* (MRL/lpr) and C3H/HeJ-*lpr*/*lpr* (C3H/lpr) mice[23,24]. MXH10/Mo/lpr mice were bred under pathogen-free conditions at Animal Research Institute, Tohoku University. These mice exhibit systemic lymphadenopathy. At 3 months of age, LNs in these mice enlarge to 10 mm in diameter, a size similar to that of human LNs. This feature makes it possible to reliably perform experiments using murine LNs. In this experiment, to study LN metastasis two LNs were utilized, which are upstream of the subiliac LN (SiLN) and its downstream of the proper axillary LN (PALN). The experimental protocol was approved by the Institutional Animal Care and Use Committee of Tohoku University. All methods were reported in compliance with the ARRIVE guidelines. All in vivo experimental procedures were conducted using the inhalation of 2% isoflurane (Pfizer Inc., New York, United States) in oxygen. Mice were euthanized by cervical dislocation under isoflurane anesthesia at the end of the experiments.

Cell line

FM3A-Luc (luciferase gene expressing mouse breast cancer) cells[23,25] were cultured in RPMI-1640 (Sigma-Aldrich, St. Louis, MO, USA) supplemented with 10% fetal bovine serum (FBS; Sigma-Aldrich), 1% L -glutamine-penicillin–streptomycin (FUJIFILM Wako Pure Chemical Industries, Osaka, Japan) and 0.5 mg/mL Geneticin (G418; FUJIFILM Wako Pure Chemical Industries) under 37 °C, 5% CO2. The medium was changed every 3 to 4 days. Cells were routinely checked for mycoplasma contamination using a detection kit (R&D System Inc., Minneapolis, MN, USA) and used for experiments after three passages.

Creating tumor bearing LN mouse model

Tumor cell suspension was prepared by adjusting the volume of 3.3×10^5 cells/mL using PBS (Sigma-Aldrich) and Matrigel (Collaborative Biochemical Products, Bedford, MA, USA) in a 3:1 volume ratio. 60 µL of cell suspension was inoculated into right SiLN of MXH10/Mo/lpr mouse to induce metastasis in the PALN.

Injection of carboplatin under the different conditions

Six experimental groups, using constant osmotic pressure, with varied viscosity, number of doses and injection rate were prepared (Table 1)—Placebo group ($n = 11$), 1897G SB (one dose of solvent with an 1897 kPa of osmotic pressure and 1 mPa·s of viscosity at bolus) group ($n = 8$), 1897G DB (two doses of solvent with an 1897 kPa of osmotic pressure and 1 mPa·s of viscosity at bolus) group ($n = 10$), 1897P SB (one dose of solvent with an 1897 kPa of osmotic pressure and 12 mPa·s of viscosity at bolus) group ($n = 5$), 1897P S10 (one dose of solvent with an 1897 kPa of osmotic pressure and 12 mPa·s of viscosity at 10 µL/min) group ($n = 4$), 1897P DB (two doses of solvent with an 1897 kPa of osmotic pressure and 12 mPa·s of viscosity at bolus) group ($n = 10$), 1897P D10 (two doses of solvent with an 1897 kPa of osmotic pressure and 12 mPa·s of viscosity at 10 µL/min) group ($n = 10$).

In these groups, treatment was performed 4 days or 4 and 6 days after tumor cell inoculation (Fig. 1).

For Placebo group, saline (Otsuka Pharmaceutical Company, Tokyo, Japan) was adjusted to 1897 kPa of osmotic pressure and 1 mPa·s of viscosity using glucose (Otsuka Pharmaceutical Company) and distilled water. For the treatment group, carboplatin (CBDCA; FUJIFILM Wako Pure Chemical Industries) was administered at 200 µL with final concentration of 15 mg/kg. The group of 1897 kPa of osmotic pressure and 1 mPa·s of viscosity formulation was diluted with glucose (Otsuka Pharmaceutical Company), saline (Otsuka Pharmaceutical Company) and distilled water. The group of 1897 kPa of osmotic pressure and 12 mPa·s of viscosity formulation was diluted with polysorbate 80 (NOF, Tokyo, Japan), saline (Otsuka Pharmaceutical Company), 100% ethanol (FUJIFILM Wako Pure Chemical Industries) and distilled water. Osmotic pressure and viscosity were determined from previous studies and adjusted based on theoretical values[12–15]. To monitor drug retention, 100 µg/mL of ICG solution (Daiichi Sankyo Co., Tokyo, Japan) was mixed with CBDCA for all experimental groups.

Evaluation of drug retention

In vivo ICG fluorescent intensity was measured using in vivo bioluminescence/biofluorescent imaging system (IVIS, Perkin Elmer, Inc, Waltham, MA, USA). The retention of administered drug was monitored on days 4, 6, 8, 11, 18, 21, 28, 35 and 42 after inoculation (Fig. 1). Biodistribution of carboplatin was a quantified expression of 195Pt using inductively coupled plasma mass spectroscopy (ICP-MS) according to previously mentioned protocol[14]. Briefly, in 1897 kPa osmotic pressure, Carboplatin with different viscosity solutions was injected via LDDS into tumor -free mice on Day 0 ($D0^T$). Pt concentration in the SiLN, PALN, lung, liver, and kidney were quantified on day 0 and/or day 9 after treatment. Pt retention per organ was calculated with $D0^T/D9^T \times 100\%$.

Evaluation of tumor growth

Tumor growth after treatment was assessed by measuring in vivo bioluminescence intensity around the PALN and tumor inoculated SiLN using IVIS. 15 mg/mL of luciferin (D-Luciferin Potassium Salt, Cayman chemical, MI, USA) was injected intraperitoneally at 10 µL/g after mice were weighed. Bioluminescence intensity was measured 10 min after intraperitoneal (i.p.) injection, and exposure time was 60 s. The in vivo bioluminescence

intensity was measured on days 4, 6, 8, 11, 18, 21, 28, 35 and 42 after inoculation (Fig. 1). The measurement of the 1897P DB group ended at a different time point because tumor growth leading to lymphatic obstruction was observed after day 21, requiring measurement completion by day 18. In the placebo group, the day 6 measurement was not conducted. The ex vivo bioluminescent intensity of liver, lung, SiLN and PALN were measured on day 42 after tissue removal. Bioluminescence per unit time was calculated using the provided analysis software (Living Image; Perkin Elmer). Metastasis induction was confirmed if luciferase intensity exceeded the background level ($5 \times 10\text{^}5$ p/s/cm2/sr).

LN volume measurement

Tumor growth after treatment was observed by measuring LN volume using a small animal high-frequency ultrasound imaging system (VEVO770; FUJIFILM Visual Sonics, Tokyo, Japan). An ultrasound gel (Parker laboratories Inc., Fairfield, NJ, USA) was placed over the LNs of the mouse, and an ultrasound probe (RMV-704; center frequency 40 MHz, spatial resolution 40 μm, azimuthal resolution 80 μm) connected to a 3D stage controller system was placed. The probe was fixed at the position of the largest segment of each LN. Ultrasound images of LNs were taken in B-mode on days 0, 4, 8, 11, 18, 21, 28, 35 and 42 after inoculation (Fig. 1), and 3D images were reconstructed using VEVO software (VEVO 770 V3.0.; FUJIFILM, Visual Sonics) with the acquired 2D images. LN volumes were calculated from the 3D images, and LN volume changes after tumor cell inoculation were evaluated by normalizing the LN volumes of PALN and SiLN on day 0 as a reference.

Histopathological analysis

On day 42, SiLN, PALN, lung, and liver were removed, and formalin fixed paraffin embedded tissues were prepared, and 2.5 μm thin sections were made to prepare histopathology specimens. SiLN, PALN, lung and liver sections were stained with Hematoxylin and Eosin (HE). Lung tissues were also stained with Elastica Masson (EM)[26], and analyzed in each experimental group. Tumor growth in LNs graded based on Table S1.

Quantitative reverse transcription-PCR (qRT-PCR)

Spleens of Placebo, 1897G SB, 1897P S10, 1897G DB and 1897P D10 groups were removed from the mice on day 10 and 42 and immersed in RNAlater (Sigma Aldrich). Each tissue was homogenized, and mRNAs were isolated using FastGene RNA Premium Kit (Nippon Genetics Co., Ltd, Tokyo, Japan). The concentration of isolated mRNAs was measured using a spectrophotometer (NanoDrop ND 1000, Thermo Fisher Scientific, Waltham, MA, USA) and adjusted to a concentration of 100 ng/μL mRNA. First, standard cDNA was synthesized with a high-capacity cDNA reverse transcription kit (4,374,966, Applied Biosystems, Foster City, CA, USA) containing RNase inhibitor. The expression levels of cell surface antigens (CD4, CD8) and cytokines (IL-6, IL-10, IL-12α, IL-12β, TNF-α, IFN-γ) were measured according to the nucleotide sequences for primers and probes are listed in Table S2. The expression levels in the carboplatin-treated group were normalized to those in the Placebo group.

Statistical analysis

The results in this study are shown as mean ± standard error. Statistical analysis and graphing were performed using statistical software (GraphPad Prism 8; GraphPad Software, Inc.). The significance tests were performed using one-way ANOVA, Tukey's multiple comparison test, 2-way ANOVA, Tukey's multiple comparison test, and uncorrelated t-test. $^{****}P < 0.0001$, $^{***}P < 0.001$, $^{**}P < 0.01$, and $^{*}P < 0.05$ are statistically significant differences.

Data availability

Data supporting this study's findings are available from the K.T. upon reasonable request.

Received: 20 February 2025; Accepted: 21 April 2025
Published online: 08 May 2025

References

1. Pantel, K. & Brakenhoff, R. H. Dissecting the metastatic cascade. *Nat. Rev. Cancer.* **4**, 448–456 (2004).
2. Cao, Y. Opinion: Emerging mechanisms of tumour lymphangiogenesis and lymphatic metastasis. *Nat. Rev. Cancer.* **5**, 735–743 (2005).
3. Mumprecht, V. & Detmar, M. Lymphangiogenesis and cancer metastasis. *J. Cell Mol. Med.* **13**, 1405–1416 (2009).
4. Xie, Y., Bagby, T. R., Cohen, M. S. & Forrest, M. L. Drug delivery to the lymphatic system: Importance in future cancer diagnosis and therapies. *Expert Opin. Drug Deliv.* **6**, 785–792 (2009).
5. Mikada, M. et al. Evaluation of the enhanced permeability and retention effect in the early stages of lymph node metastasis. *Cancer Sci.* **108**, 846–852 (2017).
6. Swartz, M. A. The physiology of the lymphatic system. *Adv. Drug Deliv. Rev.* **50**, 3–20 (2001).
7. Miura, Y. et al. Early diagnosis of lymph node metastasis: Importance of intranodal pressures. *Cancer Sci.* **107**, 224–232 (2016).
8. Jeong, H. S. et al. Investigation of the lack of angiogenesis in the formation of lymph node metastases. *J. Natl. Cancer Inst.* https://doi.org/10.1093/jnci/djv155 (2015).
9. Kodama, T., Matsuki, D., Tada, A., Takeda, K. & Mori, S. New concept for the prevention and treatment of metastatic lymph nodes using chemotherapy administered via the lymphatic network. *Sci. Rep.* **6**, 32506 (2016).
10. Tada, A., Horie, S., Mori, S. & Kodama, T. Therapeutic effect of cisplatin given with a lymphatic drug delivery system on false-negative metastatic lymph nodes. *Cancer Sci.* **108**, 2115–2121 (2017).
11. Fujii, H. et al. Treatment of false-negative metastatic lymph nodes by a lymphatic drug delivery system with 5-fluorouracil. *Cancer Med.* **8**, 2241–2251 (2019).
12. Sukhbaatar, A., Mori, S. & Kodama, T. Intranodal delivery of modified docetaxel: Innovative therapeutic method to inhibit tumor cell growth in lymph nodes. *Cancer Sci.* **113**, 1125–1139 (2022).
13. Sukhbaatar, A., Mori, S., Shiga, K. & Kodama, T. Intralymphatic injection of chemotherapy drugs modulated with glucose improves their anticancer effect. *Biomed. Pharmacother.* **165**, 115110 (2023).

14. Mishra, R. et al. Drug formulation augments the therapeutic response of carboplatin administered through a lymphatic drug delivery system. *Cancer Sci.* **114**, 259–270 (2023).
15. Sukhbaatar, A., Mori, S., Sugiura, T. & Kodama, T. Docetaxel administered through a novel lymphatic drug delivery system (LDDS) improved treatment outcomes for lymph node metastasis. *Biomed. Pharmacother.* **171**, 116085 (2024).
16. Lokich, J. & Anderson, N. Carboplatin versus cisplatin in solid tumors: an analysis of the literature. *Ann. Oncol.* **9**, 13–21 (1998).
17. Sousa, G. F. D., Wlodarczyk, S. R. & Monteiro, G. Carboplatin: molecular mechanisms of action associated with chemoresistance. *Braz. J. Pharm. Sci.* **50**, 693–701 (2014).
18. Zhang, C., Xu, C., Gao, X. & Yao, Q. Platinum-based drugs for cancer therapy and anti-tumor strategies. *Theranostics.* **12**, 2115–2132 (2022).
19. Oh, G. S. et al. Cisplatin-induced kidney dysfunction and perspectives on improving treatment strategies. *Electrolyte Blood Press.* **12**, 55–65 (2014).
20. Miller, R. P., Tadagavadi, R. K., Ramesh, G. & Reeves, W. B. Mechanisms of Cisplatin nephrotoxicity. *Toxins (Basel).* **2**, 2490–2518 (2010).
21. Galluzzi, L., Humeau, J., Buque, A., Zitvogel, L. & Kroemer, G. Immunostimulation with chemotherapy in the era of immune checkpoint inhibitors. *Nat. Rev. Clin. Oncol.* **17**, 725–741 (2020).
22. Oguri, S. et al. Clinical pharmacokinetics of carboplatin. *J. Clin. Pharmacol.* **28**, 208–215 (1988).
23. Shao, L. et al. Lymphatic mapping of mice with systemic lymphoproliferative disorder: Usefulness as an inter-lymph node metastasis model of cancer. *J. Immunol. Methods.* **389**, 69–78 (2013).
24. Tanaka, Y. et al. Evaluating the role of rheumatoid factors for the development of rheumatoid arthritis in a mouse model with a newly established ELISA system. *Tohoku J. Exp. Med.* **220**, 199–206 (2010).
25. Song, W. et al. Comprehensive studies of pharmacokinetics and biodistribution of indocyanine green and liposomal indocyanine green by multispectral optoacoustic tomography. *RSC Adv.* **5**, 3807–3813 (2015).
26. Sukhbaatar, A., Sakamoto, M., Mori, S. & Kodama, T. Analysis of tumor vascularization in a mouse model of metastatic lung cancer. *Sci. Rep.* **9**, 16029 (2019).
27. Fujii, H., Horie, S., Takeda, K., Mori, S. & Kodama, T. Optimal range of injection rates for a lymphatic drug delivery system. *J Biophotonics.* **11**, e201700401 (2018).
28. St Paul, M. & Ohashi, P. S. The roles of CD8(+) t cell subsets in antitumor immunity. *Trends Cell Biol.* **30**, 695–704 (2020).
29. Croft, M., Carter, L., Swain, S. L. & Dutton, R. W. Generation of polarized antigen-specific CD8 effector populations: Reciprocal action of interleukin (IL)-4 and IL-12 in promoting type 2 versus type 1 cytokine profiles. *J. Exp. Med.* **180**, 1715–1728 (1994).
30. Chan, W. L., Pejnovic, N., Lee, C. A. & Al-Ali, N. A. Human IL-18 receptor and ST2L are stable and selective markers for the respective type 1 and type 2 circulating lymphocytes. *J. Immunol.* **167**, 1238–1244 (2001).
31. Yang, Y., Ochando, J. C., Bromberg, J. S. & Ding, Y. Identification of a distant T-bet enhancer responsive to IL-12/Stat4 and IFNgamma/Stat1 signals. *Blood* **110**, 2494–2500 (2007).
32. Dijkgraaf, E. M. et al. Chemotherapy alters monocyte differentiation to favor generation of cancer-supporting M2 macrophages in the tumor microenvironment. *Cancer Res.* **73**, 2480–2492 (2013).

Acknowledgements
Not applicable.

Author contributions
MM: Investigation, Data curation, Formal analysis, Visualization, Writing- Original draft preparation; AS: Data curation, Visualization, Funding acquisition, Writing- Original draft preparation, Review and Editing, Supervision; RM: review and Editing; AD: Investigation; SM: Validation, Formal analysis, Writing – review and editing, Supervision; TK: Conceptualization, Methodology, Validation, Project administration, Writing – review and editing, Supervision, Funding acquisition. The authors have read and approved the manuscript.

Funding
The study was supported by JSPS KAKENHI grant numbers 20K20161 (AS), 22K18203 (AS), 21K18319 (TK), and 23H00543 (TK). Suzuken Memorial Foundation (AS).

Declarations

Competing interests
The authors declare no competing interests.

Ethics approval
Approval of the research protocol by an Institutional Reviewer Board. Approval obtained from the Institutional Animal Care and Use Committee of Tohoku University Animal Studies: All investigations carried out using murine models, including the ARRIVE protocol, were compliant with the guidelines of the Institutional Animal Care and Use Committee of Tohoku University.

Additional information
Supplementary Information The online version contains supplementary material available at https://doi.org/10.1038/s41598-025-99602-8.

Correspondence and requests for materials should be addressed to T.K.